Exploring Fluorescent Dyes at Biomimetic Interfaces with Second Harmonic Generation and Molecular Dynamics

Giuseppe Licari,[†] Lukasz Cwiklik,[‡] Pavel Jungwirth,[§] and Eric Vauthey[*,†]
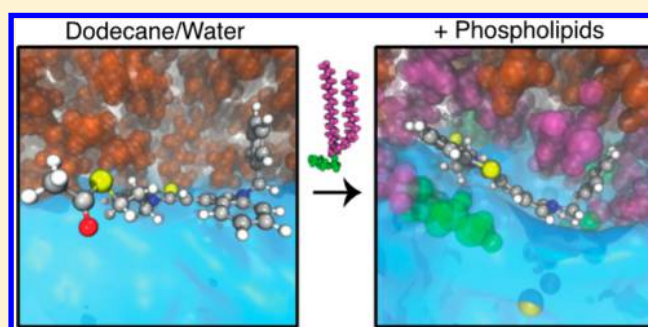
[†]Department of Physical Chemistry, University of Geneva, 30 quai Ernest-Ansermet, CH-1211 Geneva 4, Switzerland
[‡]J. Heyrovský Institute of Physical Chemistry, Czech Academy of Sciences, Dolejškova 2155/3, 182 23 Prague 8, Czech Republic
[§]Institute of Organic Chemistry and Biochemistry, Czech Academy of Sciences, Flemingovo nam. 2, 16610 Prague 6, Czech Republic

Ⓢ *Supporting Information*

ABSTRACT: The adsorption of a DNA fluorescent probe belonging to the thiazole orange family at the dodecane/water and dodecane/phospholipid/water interfaces has been investigated using a combination of surface second harmonic generation (SSHG) and all-atomistic molecular dynamics (MD) simulations. Both approaches point to a high affinity of the cationic dye for the dodecane/water interface with a Gibbs free energy of adsorption on the order of −45 kJ/mol. Similar affinity was observed with a monolayer of negatively charged DPPG (1,2-dipalmitoyl-*sn*-glycero-3-phospho-*rac*-(1-glycerol)) lipids. On the other hand, no significant adsorption could be found with the zwitterionic DPPC (1,2-dipalmitoyl-*sn*-glycero-3-phosphocholine) lipids. This was rationalized in terms of Coulombic interactions between the monolayer surface and the cationic dye. The similar affinity for the interface with and without DPPG, despite the favorable Coulombic attraction in the latter case, could be explained after investigating the interfacial orientation of the dye. In the absence of a monolayer, the dye adsorbs with its molecular plane almost flat at the interface, whereas in the presence of DPPG it has to intercalate into the monolayer and adopt a significantly different orientation to benefit from the electrostatic stabilization.

INTRODUCTION

Liquid/water interfaces are ubiquitous in nature and also play key roles in many technological processes.[1−3] Because of the asymmetry of forces they experience, molecules in the interfacial region tend to adopt an orientation that is no longer isotropic, contrary to those in the bulk phase. This confers to these interfaces properties that substantially depart from those of the two constituting bulk liquids.[4−11] As a consequence, chemical reactivity in such an environment may substantially differ from that in the solution phase.[12] This is exploited in the so-called on-water organic synthesis, where reactions of hydrophobic reactants are strongly accelerated in the presence of water.[13−16] The latter effect is due to not only the specific properties of the interface itself but also the anisotropic orientation of the adsorbed molecules, which can strongly facilitate intermolecular reactions with low steric factors. Similarly, the interfacial orientation of the adsorbates can enhance or prevent their aggregation relative to bulk solutions.[17−20]

This orientation strongly depends on the structure of the adsorbate, on the presence of hydrophilic and lipophilic groups as well as on their location on the molecule. The presence and the nature of these groups also significantly affect the affinity of the molecule toward the interface. The adsorption of charged molecules at the interface can be influenced by the addition of salts to the aqueous phase.[21−24] For example, the concentration

of cationic dye malachite green at the alkane/water interface increases remarkably upon adding a salting-in anion such as thiocyanate.[24] This is due to the excess concentration of these anions in the interfacial region relative to the bulk[25−27] and thus to the Coulombic attraction of the oppositely charged dye. A similar effect was reported with anionic surfactant sodium dodecyl sulfate (SDS) but only at concentrations lower than that required to form a monolayer.[28] Indeed, at higher SDS concentrations, this enhancement effect totally vanished and the population of absorbed dye was apparently similar to that without any surfactant. This was explained in terms of the competition for adsorption between the dye and SDS, which is strongly in favor of the latter given its strong amphiphilic nature. However, the effect of the presence of a surfactant monolayer at the interface on the adsorption of the dye was not further investigated. Such knowledge is particularly useful for our understanding of the interactions between the surfaces of membranes and molecules dissolved in the subphase.

We report here on our investigation of the adsorption properties of a dye in the presence of phospholipid monolayers at the dodecane/water interface. Because phospholipids are the main constituents of cell membranes, such a dodecane/
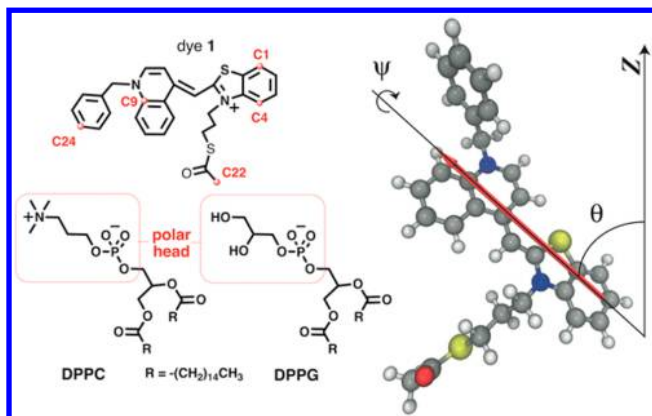
phospholipid/water combination can be considered to be a simple but valuable model for investigating the interactions between the surfaces of biological membranes and water-soluble molecules. As a dye, we chose cyanine dye **1** (Chart 1),[29] which belongs to the thiazole orange (TO) family of

Chart 1. Structures of Dye and Phospholipids[a]

[a](Left) Structure of dye **1** and of the DPPC and DPPG phospholipids. (Right) Three-dimensional representation of dye **1**, with the $S_1 \leftarrow S_0$ transition dipole moment (red arrow) and the Euler angles, θ and ψ. (See the text.) The Z axis is normal to the interfacial plane.

fluorescent DNA probes. This dye is also closely related to the yellow oxazole (YO) DNA-probe family,[30,31] several of which have recently been shown to have a high affinity for the dodecane/water interface.[32,33] This affinity can be understood by considering that these DNA probes are soluble in water but have a high binding constant to DNA upon intercalation into the hydrophobic base-pair stack. The selected phospholipids are DPPC and DPPG (Chart 1), which have zwitterionic and anionic heads, respectively, whereas **1** bears a single positive charge. This allows the influence of Coulombic effects in the adsorption of the dye to be studied.

For this investigation, we combined surface second harmonic generation (SSHG) and molecular dynamics (MD) simulations. SSHG is intrinsically surface-selective because the signal is directly proportional to the square modulus of the second-order susceptibility, $\chi^{(2)}$, which vanishes in centrosymmetric media, within the dipolar approximation.[34,35] Moreover, the SSHG signal is significantly resonantly enhanced when the probing wavelength coincides with one- or two-photon electronic transitions. This allows the selective detection of adsorbates at low concentrations without interference due to the nonresonant signal originating from the interface itself.[36] Furthermore, information on the orientation of the adsorbed molecules can be inferred from the analysis of polarization-resolved SSHG measurements.[37−39] Previous SSHG studies of liquid-supported surfactant monolayers have been mostly performed at air/liquid interfaces and were often directly probing the monolayer itself.[39−44] Similar direct probing of phospholipid monolayers at liquid interfaces was performed by vibrational sum-frequency generation (SFG).[11,45−53] The study presented here differs substantially from the previous ones because probing is done on the adsorbate, i.e., **1**, and not on the monolayer.

The absolute orientation of the dyes and the distribution of their orientation at the interface cannot be deduced from the SSHG data. This information was obtained here by performing

atomistic MD simulations of **1** at the different interfaces. The aim of these simulations was also to rationalize the SSHG data and to obtain a microscopic picture of the interactions between the dye and these interfaces. Such a combination of SSHG spectroscopy and MD simulations is relatively well established.[54−60] However, to the best of our knowledge, it has never been applied to interfaces with phospholipid monolayers.

■ METHODS

Samples. Dye **1**, 1-benzyl-4-[(3-(3-acetylsulfanylpropyl)-2(3*H*)-benzothiazol-2-ylidene)methyl]quinolinium iodide, was obtained from T. Deligeorgiev (Faculty of Chemistry, University of Sofia) and used as received. It was synthesized as described in ref 29 and recrystallized from ethanol. Its purity was checked by comparing its absorption and fluorescence excitation spectra. The samples were freshly prepared from a 2 mM stock solution of dye in dimethyl sulfoxide (Acros Organics, spectroscopic grade). Dodecane (99+%) was purchased from Alfa Aesar. DPPC (1,2-dipalmitoyl-*sn*-glycero-3-phosphocholine) and DPPG (1,2-dipalmitoyl-*sn*-glycero-3-phospho-*rac*-(1-glycerol) sodium salt) were purchased from Sigma-Aldrich.

The SSHG samples for the dodecane/water interface experiments were prepared by (a) pouring 10 mL of an aqueous dye solution into a $4 \times 4 \times 4$ cm³ quartz cell and then (b) slowly adding 12 mL of dodecane. For the experiments with phospholipids, a specific amount of phospholipid was slowly deposited onto the lower aqueous phase with a syringe after step (a). The phospholipids were previously solubilized at 1 mM in a CHCl₃/methanol mixture (9/1 by volume). The area per lipid was estimated from the surface pressure−area isotherms provided in the literature and recorded at air/buffer solution interfaces.[61] The pressure−area isotherms of phospholipids at air/water and oil/water interfaces were recently shown to be similar.[62] However, the area per lipid is only approximate because the total area of the sample in the quartz cell could not be determined precisely as a result of the meniscus.

For concentration-dependent SSHG measurements, the concentration was changed in situ by adding varying amounts of dye to the sample with a syringe, and the final concentration was corrected for the dilution. The sample was stirred with a tiny magnetic stirrer for about 5 min after each dye addition. Because the number of adsorbed molecules is proportional to the amplitude of the second-harmonic field, then the square root of the SSHG intensity was taken and the maximum of the resulting signal vs concentration curve was normalized to 1, the maximum surface coverage. All experiments were performed at 294 ± 2 K.

Surface Second Harmonic Generation. The SSHG setup has been described in detail previously.[20,33] The probe pulses (∼100 fs, ∼0.7 μJ) centered at 1020 nm were generated by a collinear optical parametric amplifier (TOPAS-C, Light Conversion) pumped by the output of a Ti:sapphire amplifier (Solstice, Spectra-Physics). This wavelength is close to the maximum in a SSHG band of **1**, which originates from two-photon resonance with the $S_1 \leftarrow S_0$ transition.[32] The probe pulses were focused on the sample by a 400 mm lens and hit the sample under the total internal reflection condition with an angle of incidence of about 70°. The quadratic dependence of the signal was checked to ensure the absence of higher-order processes (Figure S13, Supporting Information). No signal coming from the pure dodecane/water or dodecane/phospholipids/water interfaces could be detected in the absence of dye. The polarization of the probe beam was controlled with a half-wave plate, whereas the p (0°), s (90°), or m (45°) polarization components of the second-harmonic signal were selected using a wire-grid polarizer. An analysis of the polarization-resolved SSHG data was done as discussed previously[33] and is described in detail in the Supporting Information.

Molecular Dynamics Simulations. Classical MD simulations were performed using the GROMACS 5.1.2 software.[63] The fully atomistic AMBER99SB-ILDN force field (FF) was employed.[64,65] The standard TIP3P model was used for water,[66] whereas the phospholipids were described with the SLipids parameter set.[67,68] Initial GROMACS topology files for dodecane and **1** based on the

AMBER force field were automatically generated by the Antechamber tool,[69] providing the Merz−Singh−Kollman electrostatic potential[70] used to obtain the partial charges in the restricted electrostatic potential approach (RESP).[71] The force field parameters of **1** were further refined using electronic structure calculations (SI). For dodecane, Antechamber generated by default only two atom types, one for carbon and one for hydrogen. Because the default value of the Lennard-Jones potential depth ε was too large, dodecane was freezing at room temperature within 100 ns. Therefore, the dodecane atom types were changed to have parameters ε and σ matching those from the work by Jambeck and Lyubartsev,[68] where two different sets of carbon and hydrogen types were used for the CH_3 and CH_2 groups.

A periodic rectangular box containing two distinct interfaces was used for the simulations (Figure 1). The exact number of molecules in
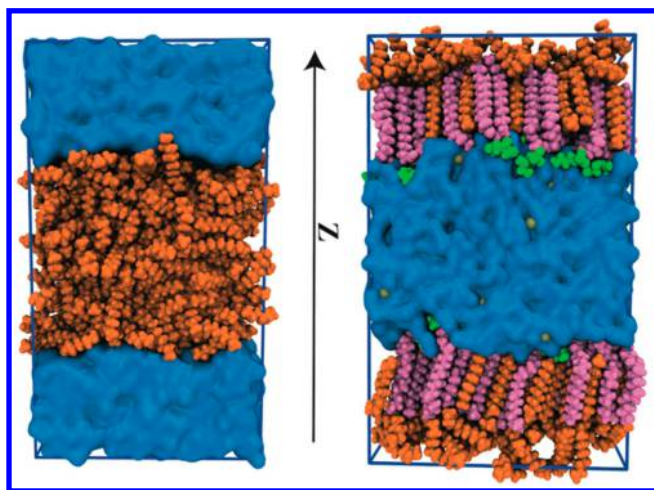

Figure 1. Examples of unit cells used for the MD simulations: dodecane/water (left) and dodecane/phospholipid/water (right). Each simulation box contains two distinct interfaces (blue, water; orange, dodecane; magenta, phospholipid tails; green, phospholipid heads; and tan, partially visible counterions).

each simulation can be found in the Supporting Information (Table S2) together with other details about the isothermal−isobaric ensembles used in the simulations. Nonbonded interactions were evaluated with a cutoff of 1.4 nm, and long-range interactions were accounted for by the particle mesh Ewald method,[72] with 0.12 nm grid spacing and forth-order interpolation. A long-range dispersion correction for energy was also included. The LINCS algorithm[73] was used to constrain the bonds of all system components with the exception of water, for which the SETTLE algorithm was applied.[74] The time step was set to 2 fs. Simulations were run for 200−600 ns, and the first 100 ns was always considered to be an equilibration period. The equilibration of the system was ensured by inspecting the total energy drift, the dye contacts with the interface, and the density profiles at the two distinct interfaces of the box.

The Gibbs free energies of adsorption and of dimerization of **1** were deduced from one-dimensional potentials of mean force (PMF)[75] obtained using the umbrella sampling technique.[76−78] The reaction coordinate for the binding of the dye at the interface was the Z axis of the simulation box. The reference species were the center of mass (COM) of dodecane and DPPG, whose positions were already restrained with respect to the Z axis because neither dodecane nor DPPG is soluble in water. Each COM pull simulation was started after an equilibration MD, which terminated with the dye adsorbed at the interface. In the case of the dodecane/DPPG/water system, the area per DPPG was fixed to 70 Å^2, and **1** was found to intercalate into the DPPG monolayer, as discussed below.

In the case of the dimerization of **1**, a preliminary MD simulation was performed in pure water with two separate dye molecules. After a few nanoseconds, a stable dimer of **1** was formed and a suitable snapshot was selected as a starting point for the pull simulation. Thus,

one dye molecule was constrained to its position to serve as an immobile reference, and the second dye molecule was pulled out of the dimer along the Z direction.

In all cases, the freely moving dye was pulled for hundreds of picoseconds using a spring constant of 1000 kJ mol^{-1} nm^{-2} and a pull rate of 0.01 nm ps^{-1}.[77] From the pull simulations, snapshots with a COM separation of about 0.1 nm between the two species were extracted and used as the starting point for the umbrella sampling. In each umbrella window, an MD simulation of 8 ns (for dodecane/DPPG/water) and 5 ns (for the other two systems) was performed, and the bootstrapping procedure was repeated 200 times during the weighted histogram analysis method (WHAM) analysis. The PMF path was extracted from the probability distribution along the reaction coordinate obtained by umbrella sampling using WHAM.[79,80] The statistical error was estimated using the bootstrap method, as also implemented in the GROMACS software. The error in the Gibbs free energies was retrieved from the errors at the maximum and minimum in the PMFs considering a confidence interval of two standard deviations.

Electronic Structure Calculations. Density functional theory (DFT) calculations were performed using Gaussian 09 (revision D)[81] to refine several parameters of the force field of **1** as described in detail in the SI. The optimized structure for the force field refinement was obtained at the B3LYP/6-311+G(d,p) level of theory[82] using the implicit polarized continuum model (PCM) representation for water.[83]

The vertical transition energies of **1** for the spectral simulations were calculated from time-dependent DFT (TD-DFT)[84−86] using either B3LYP or the long-range-corrected CAM-B3LYP functional[87] with the following functional parameters: $\mu = 0.33$, $\alpha = 0.15$, and $\beta = 0.37$.[33]

■ RESULTS AND DISCUSSION

Affinity of the Dye for the Interfaces. In previous studies,[32,33] the high interfacial affinity of YO DNA probes was mostly inferred from the high intensity of the SSHG signal as well as from various observations, such as the disruption of aggregates upon adsorption at the interface. Direct information is obtained here by measuring the adsorption isotherm of **1** at liquid/liquid interfaces by SSHG. Such measurements are usually performed at air/liquid interfaces,[55,88−90] but the liquid/liquid interface is a better model of the membrane environment.

The strong adsorption of **1** at both dodecane/water and dodecane/DPPG/water interfaces is demonstrated by the adsorption isotherms depicted in Figure 2. In both cases, a significant SSHG signal could already be measured at ∼0.1 μM bulk concentration of dye, with full dye coverage being
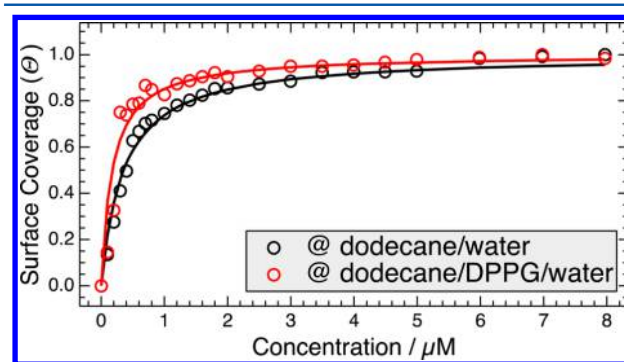

Figure 2. Adsorption isotherms of **1** at the dodecane/water and dodecane/DPPG/water interfaces measured by SSHG (66 Å^2/DPPG, 296 ± 0.5 K, m-probe polarization, s-signal polarization component). The solid lines are the best fits of the Langmuir isotherm.

achieved at around 2 μM only. By contrast, the SSHG signal measured at the dodecane/DPPC/water interface with the same area/lipid (66 Å^2/DPPC) was too weak and unstable to construct an adsorption isotherm, pointing to a much lower affinity of **1** toward this interface.

The shape of the two isotherms suggests that the simple Langmuir model can be applied here.[88,91] This model assumes that the interface is composed of identical and independent adsorption sites, which are all occupied at a surface coverage, Θ, of 1. The adsorption isotherms in Figure 2 can be safely used to determine the relative surface coverage because the orientation of the dye at both interfaces is independent of concentration as discussed below. This insures that the increase in the SSHG signal shown in Figure 2 reflects the increasing surface coverage and does not originate from changes in the second-order response due to different dye orientations.[92] The free energies of adsorption at the interfaces without and with DPPG extracted from the isotherms amount to −46.4 ± 0.3 and −48.2 ± 0.7 kJ/mol, respectively. This points to a large affinity of **1** for both interfaces. Indeed, these values are substantially larger than that reported for the adsorption of indole at the air/DPPC/water interface (−34 kJ/mol)[42] or phenol and nitrophenol at the hexane/water interfaces (around −16 kJ/mol)[37] but are comparable to that measured with *p*-decylaniline at the air/water interface (−47 kJ/mol).[88] The affinity of **1** is not strongly affected by the presence of the DPPG monolayer at the interface and increases only very modestly relative to the bare dodecane/water interface. This small difference most probably results from counteracting effects. In principle, the Coulombic attraction of cationic dye **1** toward the interface by the negatively charged heads of the DPPG monolayer should strongly favor adsorption.[21−24] However, access of **1** to the dodecane phase is largely prevented by the presence of the DPPG molecules. Moreover, the highly packed glycerol heads of DPPG may also introduce steric hindrance into the approach of **1** toward the phosphate group. The result of all of these effects is a similar affinity of **1** for both dodecane/water and dodecane/DPPG/interfaces. By contrast, the presence of DPPC at the interface has a detrimental effect on the adsorption of **1**. Compared to DPPG, DPPC has a zwitterionic head with an ammonium end group that should lead to substantial Coulombic repulsion of the cationic dye from the interface. A qualitatively similar effect of the charge of the surfactant head on the SSHG signal from ionic dyes has recently been observed.[28]

The free energy of adsorption of **1** at the dodecane/water and dodecane/DPPG/water interfaces obtained from the PMF profiles shown in Figure 3 amounts to −43.8 ± 6.6 and −48.6 ± 4.4 kJ/mol, respectively. This excellent agreement between the SSHG results and the MD simulations supports the validity of both the model and the applied force field. The MD simulations also suggest that the interfacial affinity of **1** increases slightly in the presence of DPPG, although the free-energy difference is close to the statistical error.

Figure 3 also depicts the PMF profile for the formation of dimeric aggregates of **1** in water. The resulting free energy amounts to −31.1 ± 2.4 kJ/mol, a value close to those found experimentally for similar cyanine dyes.[93−95] Therefore, even though this large free energy of dimerization points to a strong propensity toward aggregation, this process is still energetically less favorable than adsorption at the interface. This preference for adsorption over aggregation does not preclude the formation of aggregates at sufficiently high concentration, as
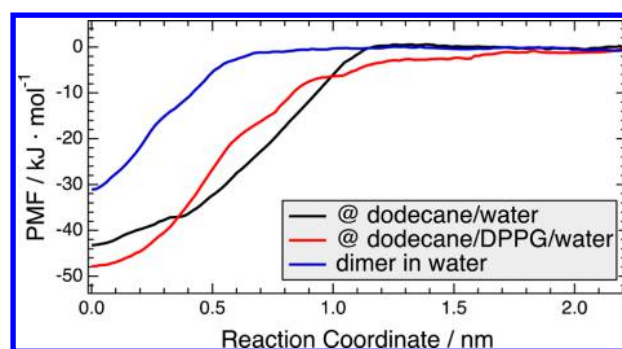

Figure 3. Potential of mean force (PMF) profiles for the adsorption of **1** at the dodecane/water and dodecane/DPPG/water interfaces (70 Å^2/DPPG) and for the aggregation of **1** into a dimer in bulk water. For better visualization, the PMF curves were arbitrarily shifted along the reaction coordinate to match the PMF minima.

shown by the MD simulations discussed below and as found experimentally with the YO equivalent of dye **1**.

Besides the Gibbs free energies, the simulations also provide insight into the interactions between the dye and the interfaces. They clearly reveal that **1** either interacts with the polar phospholipid heads from the water phase or intercalates into the phospholipid monolayer. This is illustrated in Figure 4,
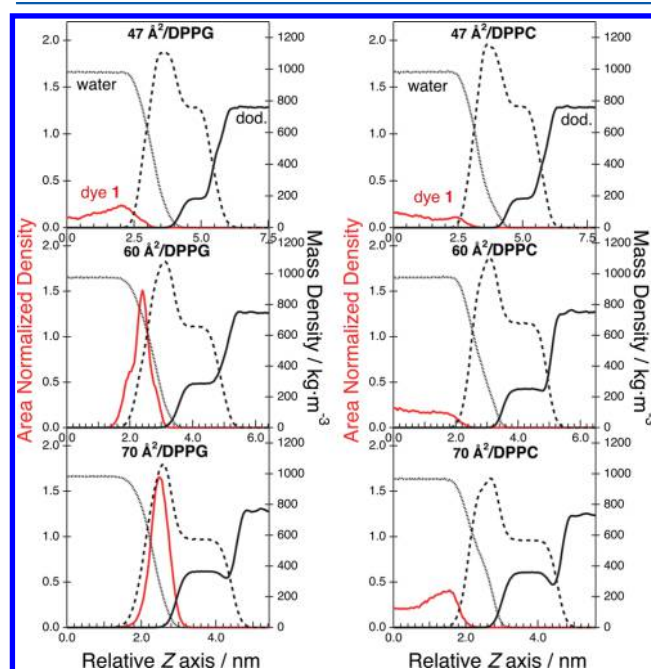

Figure 4. Density profiles obtained from simulations with a single molecule of dye **1** (red) at dodecane(solid)/phospholipid(dashed)/water(dotted) interfaces, using different areas/lipid. Left, DPPG; right, DPPC. Only one of the two interfaces of the box is shown for clarity.

where the density profiles of the individual constituents are shown for DPPG and DPPC monolayers with varying areas per phospholipid. Besides the normalized density of **1**, this figure also reports on the mass density of water, phospholipids, and dodecane along the Z axis of the unit cell. The Z = 0 value coincides with the center of the unit cell, and only half of the simulation box is shown for clarity. At high surface pressure, corresponding to a small area per lipid (47 Å^2), the dye cannot penetrate the monolayer on the time scale of the simulations. In the case of DPPG, the dye experiences an electrostatic

attraction toward the interface that favors a small accumulation at the interface relative to the bulk. It is worth noting that a fraction of dodecane molecules intercalate between the hydrophobic tails of the phospholipids and keep them in an ordered state. At lower surface pressure, i.e., at 60 Å^2/lipid, the dye starts to penetrate the DPPG monolayer but not the DPPC monolayer. The amount of dodecane intercalated between the phospholipid tails also increases. Finally, at the lowest surface pressure simulated, i.e., at 70 Å^2/lipid, the dye is fully located in the DPPG monolayer. However, with DPPC, the dye remains almost entirely in the aqueous phase and exhibits a little excess concentration close to the water/DPPC interfacial region. The orientational analysis of these dyes close to the interface points to an almost random orientation, in agreement with a weak SSHG signal (Figure S9). These results reveal that the upper dodecane phase has a significant effect on the structure of the lipid monolayer, especially at a high area per lipid. Previous MD simulations indicated that SDS tends to form aggregates at the air/water interface but not at the decane/water interface.[96] This confirms that the dodecane/phospholipid/water system is a better model of biological membranes than the air/phospholipid/water system.

The effect of surface pressure on the adsorption of **1** has also been investigated by SSHG, upon varying the area/lipid from 66 to 47 Å^2. In the case of DPPG, an intense SSHG signal from **1** was measured within this whole area/lipid range. By contrast with DPPC, an SSHG signal could be detected only at the largest area/lipid. However, as mentioned above, this signal was too weak and unstable for any reliable data to be recorded. Thus, both experiments and simulations give a very congruent picture of the adsorption behavior of **1** in the presence of a phospholipid monolayer.

Molecular Orientation at the Interfaces. Insight into the orientation of the adsorbed dye at the interfaces was obtained from polarization-resolved SSHG measurements. In these experiments, different polarization components of the SSHG signal, usually the s and p components, are recorded as a function of the polarization of the probe field, γ. As discussed in detail in the SI and in refs 35, 37, and 38, an analysis of the resulting polarization profiles allows the relative magnitude of the $\chi^{(2)}$ tensor elements to be determined. The latter depends on the hyperpolarizability tensor, β, of the species responsible for the SSHG signal (dye **1** in this case) and on its orientation

$$\chi^{(2)} \propto N\langle\beta\rangle \tag{1}$$

where N is the surface density, and the angle brackets indicate an average over the molecular orientations. Quantum-chemical calculations revealed that the hyperpolarizability tensor of a YO dye is dominated by a single element, β_{zzz}, where z is along the $S_1 \leftarrow S_0$ transition dipole moment, itself parallel to the main molecular axis.[33] We assume the same here for the structurally very similar dye **1**. In this case, the orientation parameter, D, can be calculated as

$$D = \frac{\langle\cos^3\theta\rangle}{\langle\cos\theta\rangle} = \frac{\chi^{(2)}_{ZZZ}}{\chi^{(2)}_{ZZZ} + 2\chi^{(2)}_{ZXX}} \tag{2}$$

where θ is the tilt angle, i.e., the angle between the $S_1 \leftarrow S_0$ transition dipole moment of **1** and the normal to the interface (Chart 1). $\chi^{(2)}_{ZZZ}$ and $\chi^{(2)}_{ZXX}$ are two tensor elements defined in the laboratory frame, with X and Z being in the interfacial plane and normal to the interface, respectively. In the case of a very narrow distribution of orientations, for instance, a Dirac δ

distribution, D simplifies to $\cos^2\theta$, and the tilt angle can be readily obtained from the experiment. However, such a situation where all of the molecules adsorbed at the interface adopt an identical orientation is unlikely. Therefore, a distribution has to be assumed in order to have a more realistic estimate of the mean tilt angle.

Because of the weakness of the SSHG signal with the DPPC monolayer, the polarization-resolved measurements were carried out at the dodecane/water and dodecane/DPPG/water interfaces only. An area/DPPG of 66 Å^2 was used for all measurements. As showed by the pressure−area isotherm at air/buffer interface,[61] both liquid-expanded (LE) and liquid-condensed (LC) phases coexist in the monolayer at this area/lipid, corresponding to a surface pressure of ∼10 mN/m. Because a monolayer in a highly compressed state is difficult to produce in our experiment, we chose to work in the LE/LC range.

An example of polarization-resolved data is presented in Figure 5. The ensemble of data recorded at three output
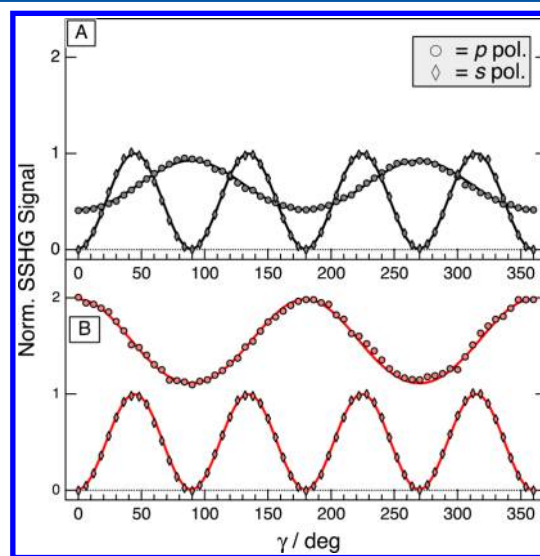

Figure 5. Polarization-resolved SSHG data recorded at two output polarizations with 2 μM dye **1** at (A) dodecane/water and (B) dodecane/DPPG/water interfaces. The solid lines are the best-fit curves of eq S5. Each set of data was normalized to the maximum of the s polarization fit curve for better comparison.

polarizations and six different dye concentrations (from 0.1 to 4 μM) is shown in Figure S11. It can immediately be seen that the polarization curves change markedly upon addition of DPPG, pointing to a different interfacial orientation of **1** in the presence of the lipid monolayer. The $\chi^{(2)}$ tensor elements extracted from these data were inserted into eq 2 to calculate the D parameter at the different concentrations (Table S5). As shown in Figure 6, D and hence the interfacial orientation of the dye at both interfaces remain constant within the whole concentration range.

The D parameters, averaged over the measurements at different concentrations, are listed in Table 1. Assuming a Dirac δ distribution of orientations, these values give tilt angles θ of approximately 60 and 50° for **1** at the dodecane/water and dodecane/DPPG/water interfaces, respectively (Table 1). The absolute direction of the dye at the interface, i.e., which of the two ends of the dye point away from the aqueous phase, cannot be inferred from the SSHG data unless heterodyne detection is
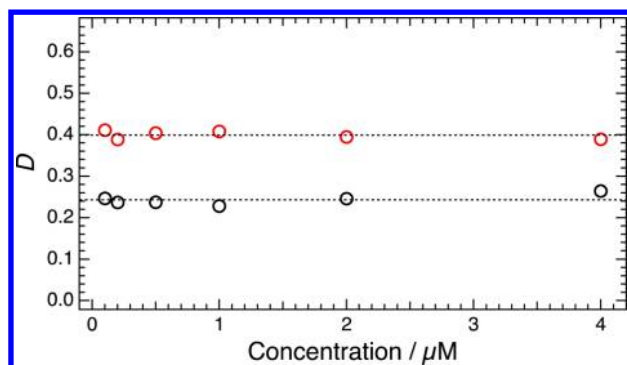
Figure 6. Orientation parameter D as a function of the bulk concentration of **1** for the dodecane/water (black) and dodecane/DPPG/water (red) interfaces. The horizontal lines pass through the average values.

Table 1. Comparison of the Experimental and Simulated Interfacial Orientations of Dye 1

	dodecane/water	dodecane/DPPG/water
experimental		
D^a	0.24 ± 0.01	0.40 ± 0.01
$\theta \, (\delta)^b$	60.5 or $119.5 \pm 0.7°$	50.8 or $129.2 \pm 0.5°$
$\theta \, (\Delta\theta)^c$	74.2 or $105.8 \pm 1.4°$	54.5 or $125.5 \pm 0.7°$
simulated		
θ	$88.7 \pm 0.2°$	$110.6 \pm 0.1°$
$\Delta\theta$	$38.0 \pm 0.5°$	$27.3 \pm 0.3°$
ψ	$87.6 \pm 0.2°$	$75.7 \pm 0.2°$
$\Delta\psi$	$48.4 \pm 0.6°$	$40.7 \pm 0.6°$

$^a D$ parameter averaged over concentration-dependent SSHG. ^{b}Calculated assuming a Dirac δ distribution. ^{c}Calculated assuming the simulated $\Delta\theta$ distribution.

performed.[97,98] Therefore, the tilt angles could also be equal to 120 and 130° without and with DPPG, respectively. The absolute orientation of **1** is difficult to predict on the basis of chemical intuition because **1** does not contain strongly hydrophilic or hydrophobic groups that could lead to a clear preferential orientation at the interface.

The smaller tilt angle with DPPG indicates that the phospholipid monolayer induces a more perpendicular orientation of the dye long axis relative to the interface. However, a Dirac δ distribution is probably not realistic. Unfortunately, the distribution of dye orientations cannot be deduced from steady-state SSHG measurements.[57,99] Therefore, we resorted to MD simulations to estimate the orientational distribution and the absolute orientation of the dye.

We present first the MD results with **1** at the dodecane/water interface. These simulations were performed at different dye concentrations to mimic the SSHG experiments. For this, the number of dye molecules initially placed in the water phase was varied between 1 and 60. After equilibration, all dye molecules were adsorbed at one of the two interfaces of the simulation box. The surface concentration was then determined from the number of molecules adsorbed at each interface and varied from 0.025 to 0.57 dye/nm². As a comparison, the lowest surface concentration used for the SSHG experiments was estimated to be about 0.3 dye/nm² using the free energy of adsorption obtained experimentally. Because the van der Waals area of the molecular plane of **1** is on the order of 1.4 nm², the

surface concentration at full coverage should be lower than ~0.7 dye/nm².

Two Euler angles, namely, the tilt angle θ and the rotational angle ψ (Chart 1), were extracted from the simulations. The rotational angle ψ is the angle between the Z laboratory axis and a vector located in the molecular plane of **1** and perpendicular to its transition dipole moment. Therefore, $\psi = 0°$ corresponds to the molecular plane being parallel to Z. The distributions of θ and ψ were analyzed using a symmetric and a skewed Gaussian function,[100] with both functions giving similar results as discussed in the SI (Figures S5 and S6). These two angles and the full width at half-maximum of their distribution, $\Delta\theta$ and $\Delta\psi$, are plotted as a function of surface concentration in Figure 7.
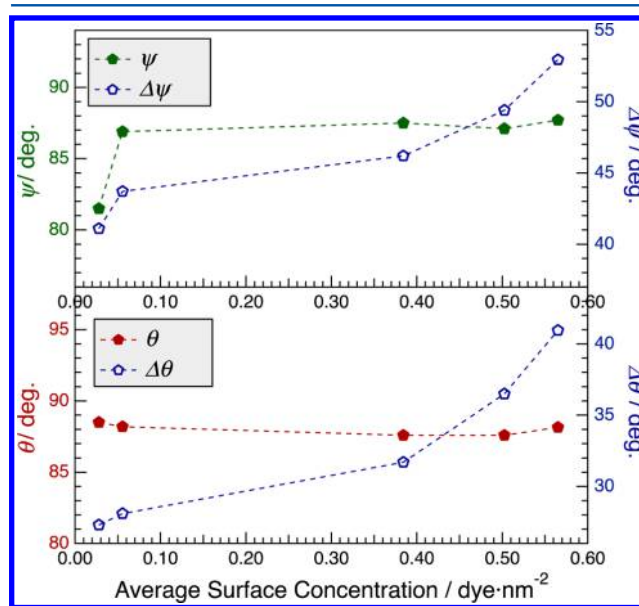

Figure 7. Orientation angles θ and ψ and corresponding distribution widths, $\Delta\theta$ and $\Delta\psi$, at the dodecane/water interface for different surface concentrations of **1** extracted from the MD simulations.

According to the simulations, the tilt angle θ is close to 90°, and because the $S_1 \leftarrow S_0$ transition dipole is essentially along the long molecular axis, **1** is lying almost flat at the interface (Figure 8A), with the benzothiazole end pointing on average slightly toward the aqueous phase. The tilt angle does not vary with concentration, in full agreement with the SSHG experiments. However, its distribution broadens from around 28 to 41° upon increasing the dye concentration. This result
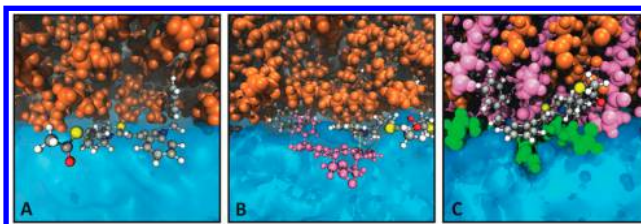

Figure 8. MD snapshots illustrating typical interfacial orientations of the dye: (A) **1** and (B) 40 dye molecules at the dodecane/water interface and (C) 1 dye molecule at the dodecane/DPPG/water interface (same color code as in Figure 1). (B) Example of transient aggregation, with a pink-colored dye molecule interacting through π-stacking with an adsorbed dye.

indicates that simulations using only one dye molecule could lead to an inaccurate description of a real system. This broadening of the distribution is due to the increased number of interactions between nearby dye molecules and the formation of transient aggregates that are in equilibrium with adsorbed monomers. These transient aggregates consist of H-type dimers with a parallel π-stacked conformation, with one constituent adsorbed at the interface as illustrated in Figure 8B. A similar concentration dependence was obtained for the distribution of the rotational angle ψ, whose width increases by almost 15° along the concentration range. The main value of ψ stabilizes at around 87° after a small initial rise from 82° upon going from one to two dye molecules. This implies that the molecular plane remains almost parallel to the interface at all concentrations.

The increase in $\Delta\theta$ with concentration deduced from the MD simulations should lead to an ∼15% increase in the D parameter, in the range of concentrations used in the experiments.[35,37,38] Such a change is close to the experimental limit of error on D and cannot be resolved here (Figure 6). However, an increase in D with increasing dye concentration was reported previously for YO derivatives.[33] There, the tilt angle was calculated from D assuming a Dirac δ distribution and was found to decrease with increasing concentration. However, the MD simulations performed here indicate that this increasing D could actually be due to an increase in $\Delta\theta$ and not to a variation of the average tilt angle.

To obtain better statistics, an MD simulation over 500 ns was performed with 40 dyes. The resulting θ and ψ values and the width of their distributions are listed in Table 1. These values are close to those extracted from the shorter simulations at a similar surface concentration. The distribution of the tilt angle obtained from this longer simulation was used to calculate the mean tilt angle from the experimentally measured D parameter. As shown in Table 1, the resulting angle amounts to 74 vs 60° as obtained by assuming a Dirac δ distribution. This angle is also closer to that found by the MD simulations (Figure 9). However, given that the tilt angle obtained from the simulation is essentially distributed around 90 °, the determination of the absolute orientation of **1** at the interface from D is not really possible. Therefore, a tilt angle distributed around 106° cannot be excluded.

The discrepancy between the experimental and MD values can be ascribed to imperfect parametrization of the dihedral angles of **1** (only three angles were refined) and/or of the force field of dodecane, both of which could lead to too flat an orientation of the dye. Nevertheless, the agreement is satisfactory, and the MD model can now be used to rationalize the orientation of the dye. The normalized densities along the Z axis of dodecane, water, and dye **1** and two of its carbon atoms, C22 and C24 (Chart 1) are reported in Figure 10A. The density profile of the C22 atom, located at the end of the long side chain of **1**, is similar to that of the center of mass of the whole dye. This indicates that the side chain does not penetrate the dodecane, although it is predominantly hydrophobic. By contrast, the density profile of C24 reveals that the benzyl is able to penetrate the dodecane phase and is most probably responsible for the slight departure of the tilt angle from 90°. This effect is observed with both 1 and 40 dye molecules in the simulation box. However, at high concentration, the density profiles associated with the dye exhibit a shoulder on the water side that is caused by the formation of transient aggregates (Figure S10).
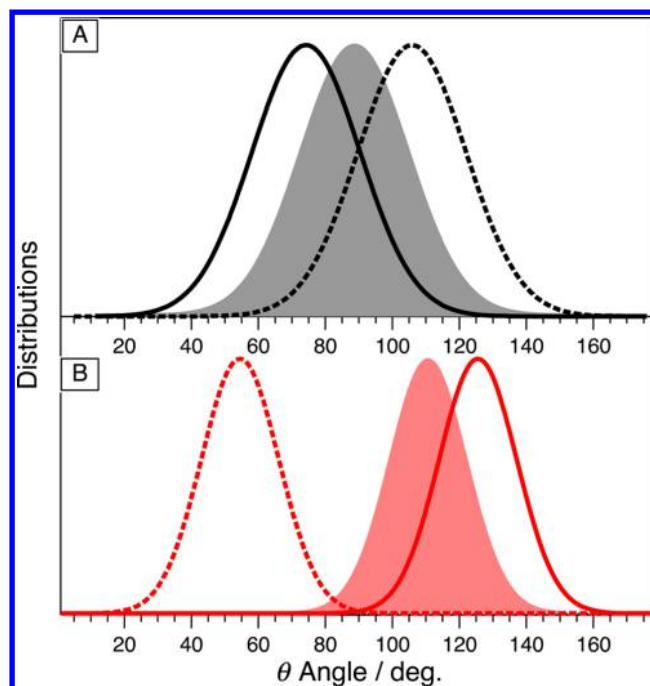

Figure 9. Comparison of the simulated (filled) and the two possible tilt angle distributions deduced from experiments (solid or dashed) of **1** at (A) dodecane/water and (B) dodecane/DPPG/water interfaces. The experimental distribution is assumed to be Gaussian, with the same width as that obtained from the simulations.
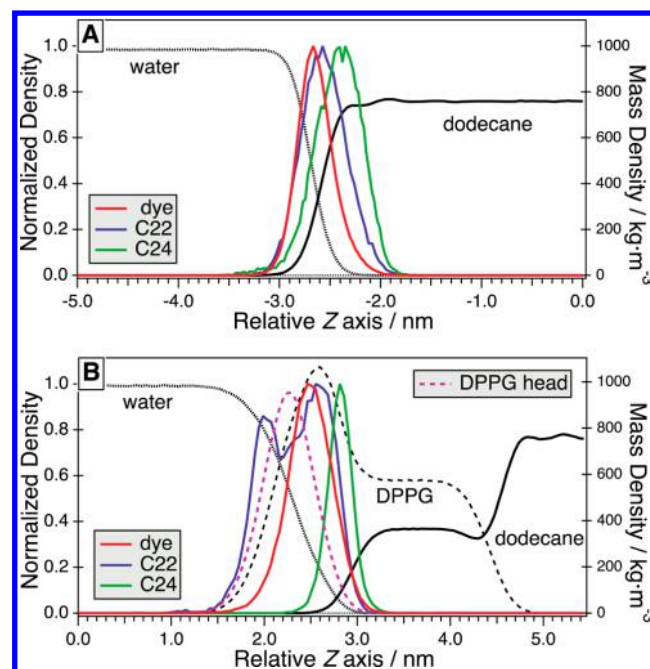

Figure 10. (A) Density profiles of water and dodecane (right axis) and normalized density of **1** and two of its atoms (left axis) for the dodecane/water system. The production MD goes from 100 to 200 ns. (B) The same as for A but for the dodecane/DPPG/water system with the density of DPPG (right axis) and the normalized density of the polar head of DPPG (left axis). The production MD goes from 100 to 300 ns. In both cases, the simulations were performed with one dye molecule. Only one interface of the box is shown for clarity.

Similar orientation analysis was carried out with the dodecane/DPPG/water interface but at only one dye

concentration because of the longer time required for the simulation. A 70 Å² area/DPPG, close to the experimental conditions, was used, and the production simulation was extended to a total time of 600 ns. In this case again, the angle distributions could be well reproduced using Gaussian functions (Figure S8). Table 1 reveals that the tilt angle of **1** in the presence of DPPG is almost 20° smaller than that predicted for the dodecane/water interface. A very similar difference is observed for the θ values determined experimentally from D. Consequently, **1** orients more perpendicular to the interface in the presence of the DPPG monolayer (Figure 8C). In this case, however, the absolute orientation of the dye is unambiguous, with the benzothiazole end clearly pointing away from the aqueous phase. The MD distribution of θ is shown in Figure 9B together with the experimental one derived from the average D parameter of 0.40 assuming a Gaussian distribution with a width of 27.3°.

The difference between the simulated and the experimental θ values is around 15° at both interfaces, suggesting a systematic error arising most probably from the parametrization of the force field. Two other effects could be at the origin of this discrepancy in the case of the dodecane/DPPG/water interface: (1) the concentration of the K^+ counterions of DPPG close to the interface is unrealistically larger in the simulations because of the very small volume of the aqueous phase in the box and (2) the estimation of the experimental surface pressure of the monolayer is only approximate. Because the dye intercalates into the monolayer, a small difference in the surface pressure could lead to a significant change in the orientation of the molecule.

The calculated normalized density profiles of **1**, C22, and C24 at the dodecane/DPPG/water interface are depicted in Figure 10B. The density profile of the polar head of DPPG is also reported for better visualization of the position of the dye in the monolayer. It appears that **1** intercalates into the monolayer and is localized just above the polar head of DPPG. This can be explained by the above-discussed Coulombic attraction of the cationic dye by the anionic polar head. In this case as well, the benzyl ring (C24) is pulled up toward the hydrophobic phase, consisting of the DPPG tails and dodecane. Despite this, the chromophoric part of the dye is oriented with the benzothiazole toward the lipophilic phase, as shown in Figure 8C. The density profile of C22 exhibits two peaks, one at 1.3 Å from the average center of mass of **1** similar to the dodecane/water interface and a second at −4.8 Å, indicating that the thioester group can also extend toward the aqueous phase and orient perpendicularly to the molecular plane of **1**. The intercalation of the dye in the monolayer should prevent the formation of transient aggregates that are observed at high dye concentration at the dodecane/water interface and that are responsible for the increase in $\Delta\theta$. Therefore, one can expect the width of the tilt angle distribution to be independent of concentration in the range used for the SSHG measurements.

Therefore, both the SSHG measurements and the MD simulations point to substantial differences in the adsorption of **1** between the two interfaces, despite very similar affinities. The MD simulations confirm that the attractive Coulombic interaction exerted by the anionic head of DPPG is somehow compensated for by the steric hindrance introduced by the lipids themselves. Therefore, the dye molecules have to intercalate into the monolayer to interact with the phosphate group of DPPG.

■ CONCLUSIONS

SSHG gives access to rich information on the adsorption of dyes at liquid interfaces and becomes particularly insightful when used in conjunction with MD simulations. This was shown here with DNA probe **1**, belonging to the well-known thiazole orange (TO) family, at three different interfaces. SSHG allows direct and specific probing of the dye at the interface, whereas fully atomistic MD simulations not only help to rationalize the experimental results but also provide a detailed molecular picture of the interface. Here two dodecane/phospholipid/water interfaces were used as a simple model of biological membranes and more specifically of their surface and were compared to the simple dodecane/water interface. The MD simulations reveal the important role of the dodecane molecules, which intercalate into the hydrophobic tails of the lipids and keep them in an ordered state even at a high area/lipid. Our results evidence the crucial role of the Coulombic interactions between the polar head of the lipids and the charged dye. The zwitterionic polar head of DPPC with the positive charge more exposed to the aqueous phase prevents the adsorption of the cationic dye. The opposite effect is observed with the negatively charged DPPG, with a high affinity of the dye toward the interface, although it is not much larger that that for the interface without phospholipid. Both polarization-resolved SSHG measurements and MD simulations point to a significant effect of DPPG on the orientation of the adsorbed dye molecules. Without phospholipid, the dye lies almost parallel to the dodecane/water interface. In the presence of DPPG, it adopts a more perpendicular orientation. Additionally, the distribution of orientations is narrower, pointing to some ordering effect. Because the latter information cannot be extracted from the SSHG measurements, the MD simulations prove to be pivotal in this respect. The modest increase in the interfacial affinity in the presence of DPPG, despite favorable Coulombic interactions, and the different orientations of the dye can be explained by the fact that in order to adsorb, the dye has to intercalate inside the monolayer, whereas it just adsorbs almost parallel to the dodecane/water interface. Consequently, the phospholipid monolayer introduces steric hindrance, which counterbalances the Coulombic attraction, and constrains the orientation of the dye.

Given the high interfacial affinity of this dye and its high binding constant to DNA, it will be particularly interesting to investigate the same systems in the presence of DNA in the aqueous phase. This could prove to be a peculiarly insightful approach toward a better understanding of membrane−DNA interactions, such as in the case of membrane-associated DNA,[101,102] whose role is still not fully understood.

■ ASSOCIATED CONTENT

ⓢ Supporting Information

The Supporting Information is available free of charge on the ACS Publications website at DOI: 10.1021/acs.langmuir.7b00403.

> Details on the force field parametrization, on the calculations of the average transition dipole moment, on the simulation boxes, on the distribution of dihedral angles, and on the orientational distributions; and additional polarization-resolved SSHG data and details of their analysis (PDF)

■ AUTHOR INFORMATION

Corresponding Author

*E-mail: eric.vauthey@unige.ch.

ORCID ●

Pavel Jungwirth: 0000-0002-6892-3288

Eric Vauthey: 0000-0002-9580-9683

Notes

The authors declare no competing financial interest.

■ REFERENCES

(1) Watarai, H.; Teramae, N.; Sawada, T. *Interfacial Nanochemistry*; Kluwer Academic: New York, 2005.

(2) Ball, P. Water as an Active Constituent in Cell Biology. *Chem. Rev.* **2008**, *108*, 74−108.

(3) Volkov, A. G. E. *Liquid Interfaces in Chemical, Biological, and Pharmaceutical Applications*; Marcel Dekker: New York, 2009.

(4) Eisenthal, K. B. Liquid Interfaces. *Acc. Chem. Res.* **1993**, *26*, 636−643.

(5) Wang, H.; Borguet, E.; Eisenthal, K. B. Polarity of Liquid Interfaces by Second Harmonic Generation Spectroscopy. *J. Phys. Chem. A* **1997**, *101*, 713−718.

(6) Steel, W. H.; Walker, R. A. Measuring Dipolar Width across Liquid-Liquid Interfaces with 'Molecular Rulers'. *Nature* **2003**, *424*, 296−299.

(7) Moore, F. G.; Richmond, G. L. Integration or Segregation: How Do Molecules Behave at Oil/Water Interfaces? *Acc. Chem. Res.* **2008**, *41*, 739−748.

(8) Fita, P.; Punzi, A.; Vauthey, E. Local Viscosity of Binary Water +Glycerol Mixtures at Liquid/Liquid Interfaces Probed by Time-Resolved Surface Second Harmonic Generation. *J. Phys. Chem. C* **2009**, *113*, 20705−20712.

(9) Fita, P.; Fedoseeva, M.; Vauthey, E. Hydrogen-Bond-Assisted Excited-State Deactivation at Liquid/Water Interfaces. *Langmuir* **2011**, *27*, 4645−4652.

(10) Richert, S.; Fedoseeva, M.; Vauthey, E. Ultrafast Photoinduced Dynamics at Air/Liquid and Liquid/Liquid Interfaces. *J. Phys. Chem. Lett.* **2012**, *3*, 1635−1642.

(11) Kundu, A.; Yamaguchi, S.; Tahara, T. Evaluation of pH at Charged Lipid/Water Interfaces by Heterodyne-Detected Electronic Sum Frequency Generation. *J. Phys. Chem. Lett.* **2014**, *5*, 762−766.

(12) Piradashvili, K.; Alexandrino, E. M.; Wurm, F. R.; Landfester, K. Reactions and Polymerizations at the Liquid−Liquid Interface. *Chem. Rev.* **2016**, *116*, 2141−2169.

(13) Breslow, R. Hydrophobic Effects on Simple Organic Reactions in Water. *Acc. Chem. Res.* **1991**, *24*, 159−164.

(14) Gajewski, J. J. The Claisen Rearrangement. Response to Solvents and Substituents: The Case for Both Hydrophobic and Hydrogen Bond Acceleration in Water and for a Variable Transition State. *Acc. Chem. Res.* **1997**, *30*, 219−225.

(15) Narayan, S.; Muldoon, J.; Finn, M. G.; Fokin, V. V.; Kolb, H. C.; Sharpless, K. B. On Water": Unique Reactivity of Organic Compounds in Aqueous Suspension. *Angew. Chem., Int. Ed.* **2005**, *44*, 3275−3279.

(16) Shapiro, N.; Vigalok, A. Highly Efficient Organic Reactions "on Water", "in Water", and Both. *Angew. Chem., Int. Ed.* **2008**, *47*, 2849−2852.

(17) Fujiwara, K.; Wada, S.; Monjushiro, H.; Watarai, H. Ion-Association Aggregation of an Anionic Porphyrin at the Liquid/Liquid Interface Studied by Second Harmonic Generation Spectroscopy. *Langmuir* **2006**, *22*, 2482−2486.

(18) Yao, H.; Ikeda, H.; Kitamura, N. Surface Induced J Aggregation of Pseudoisocyanine Dye at a Glass/Solution Interface Studied by Total-Internal-Reflection Fluorescence Spectroscopy. *J. Phys. Chem. B* **1998**, *102*, 7691.

(19) Sen, S.; Yamaguchi, S.; Tahara, T. Different Molecules Experience Different Polarities at the Air/Water Interface. *Angew. Chem., Int. Ed.* **2009**, *48*, 6439−6442.

(20) Fedoseeva, M.; Letrun, R.; Vauthey, E. Excited-State Dynamics of Rhodamine 6g in Aqueous Solution and at the Dodecane/Water Interface. *J. Phys. Chem. B* **2014**, *118*, 5184−5193.

(21) Steinhurst, D. A.; Baronavski, A. P.; Owrutsky, J. C. Transient Second Harmonic Generation from Oxazine Dyes at the Air/Water Interface. *J. Phys. Chem. B* **2002**, *106*, 3160−3165.

(22) Beildeck, C. L.; Liu, M. J.; Brindza, M. R.; Walker, R. A. Solvation of p-Nitrophenol at a Water/Alkane Interface: The Role of Ionic Strength and Salt Identity. *J. Phys. Chem. B* **2005**, *109*, 14604−14610.

(23) Punzi, A.; Martin-Gassin, G.; Grilj, J.; Vauthey, E. Effect of Salt on the Excited-State Dynamics of Malachite Green in Bulk Aqueous Solutions and at Air/Water Interfaces: A Femtosecond Transient Absorption and Surface Second Harmonic Generation Study. *J. Phys. Chem. C* **2009**, *113*, 11822−11829.

(24) Fedoseeva, M.; Fita, P.; Punzi, A.; Vauthey, E. Salt Effect on the Formation of Dye Aggregates at Liquid/Liquid Interfaces Studied by Time-Resolved Surface Second Harmonic Generation. *J. Phys. Chem. C* **2010**, *114*, 13774−13781.

(25) Jungwirth, P.; Tobias, D. J. Specific Ion Effects at the Air/Water Interface. *Chem. Rev.* **2006**, *106*, 1259−1281.

(26) Pegram, L. M.; Record, M. T., Jr Quantifying Accumulation or Exclusion of H+, Ho-, and Hofmeister Salt Ions near Interfaces. *Chem. Phys. Lett.* **2008**, *467*, 1−8.

(27) Zhang, Y.; Cremer, P. S. Chemistry of Hofmeister Anions and Osmolytes. *Annu. Rev. Phys. Chem.* **2010**, *61*, 63−83.

(28) Fedoseeva, M.; Fita, P.; Vauthey, E. Excited-State Dynamics of Charged Dyes at Alkane/Water Interfaces in the Presence of Salts and Ionic Surfactants. *Langmuir* **2013**, *29*, 14865−14872.

(29) Deligeorgiev, T.; Gadjev, N.; Vasilev, A.; Drexhage, K.-H.; Yarmoluk, S. M. Synthesis of Novel Monomeric and Homodimeric Cyanine Dyes with Thioacetyl Substituents for Nucleic Acid Detection. *Dyes Pigm.* **2006**, *70*, 185−191.

(30) Glazer, A. N.; Rye, H. S. Stable Dye-DNA Intercalation Complexes as Reagents for High Sensitivity Fluorescencec Detection. *Nature* **1992**, *359*, 859−861.

(31) Fürstenberg, A.; Deligeorgiev, T. G.; Gadjev, N. I.; Vasilev, A. A.; Vauthey, E. Structure-Fluorescence Contrast Relationship in Cyanine DNA Intercalators: Toward Rational Dye Design? *Chem. -Eur. J.* **2007**, *13*, 8600−8609.

(32) Licari, G.; Vauthey, E. Ultrafast Excited-State Dynamics at Interfaces: Fluorescent DNA Probes at the Dodecane/Water Interface. *Proc. SPIE* **2015**, *9549*, 95490M.

(33) Licari, G.; Brevet, P.-F.; Vauthey, E. Fluorescent DNA Probes at Liquid/Liquid Interfaces Studied by Surface Second Harmonic Generation. *Phys. Chem. Chem. Phys.* **2016**, *18*, 2981−2992.

(34) Eisenthal, K. B. Liquid Interfaces Probed by Second-Harmonic and Sum-Frequency Spectroscopy. *Chem. Rev.* **1996**, *96*, 1343−1360.

(35) Brevet, P.-F. *Surface Second Harmonic Generation*; Presses Polytechniques et Universitaires Romandes: Lausanne, 1997.

(36) Fedoseeva, M.; Richert, S.; Vauthey, E. Excited-State Dynamics of Organic Dyes at Liquid-Liquid Interfaces. *Langmuir* **2012**, *28*, 11291−11301.

(37) Tamburello-Luca, A. A.; Hebert, P.; Brevet, P. F.; Girault, H. H. Resonant-Surface Second-Harmonic Generation Studies of Phenol Derivatives at Air/Water and Hexane/Water Interfaces. *J. Chem. Soc., Faraday Trans.* **1996**, *92*, 3079−3085.

(38) Simpson, G. J.; Westerbuhr, S. G.; Rowlen, K. L. Molecular Orientation and Angular Distribution Probed by Angle-Resolved

Absorbance and Second Harmonic Generation. *Anal. Chem.* **2000**, *72*, 887–898.

(39) Martin-Gassin, G.; Benichou, E.; Bachelier, G.; Russier-Antoine, I.; Jonin, C.; Brevet, P. F. Compression Induced Chirality in Dense Molecular Films at the Air/Water Interface Probed by Second Harmonic Generation. *J. Phys. Chem. C* **2008**, *112*, 12958–12965.

(40) Kajikawa, K.; Takezoe, H.; Fukuda, A. Symmetry and Second-Order Susceptibility of Hemicyanine Monolayer Studied by Surface Second-Harmonic Generation. *Jpn. J. Appl. Phys.* **1991**, *30*, 1050.

(41) Teerenstra, M. N.; Hagting, J. G.; Schouten, A. J.; Nolte, R. J. M.; Kauranen, M.; Verbiest, T.; Persoons, A. Second-Harmonic Generation from Floating Monolayers and Langmuir–Blodgett Multilayers of Poly(Isocyanide)S. *Macromolecules* **1996**, *29*, 4876–4879.

(42) Mitchell, S. A. Indole Adsorption to a Lipid Monolayer Studied by Optical Second Harmonic Generation. *J. Phys. Chem. B* **2009**, *113*, 10693–10707.

(43) Matsuoka, Y.; Taguchi, D.; Manaka, T.; Iwamoto, M. Visualizing Polarization Structure of Lipid Langmuir Monolayer by Surface Second-Harmonic Generation Technique. *Thin Solid Films* **2014**, *554*, 8–12.

(44) Lv, K.; Lin, L.; Wang, X.; Zhang, L.; Guo, Y.; Lu, Z.; Liu, M. Significant Chiral Signal Amplification of Langmuir Monolayers Probed by Second Harmonic Generation. *J. Phys. Chem. Lett.* **2015**, *6*, 1719–1723.

(45) Bonn, M.; Roke, S.; Berg, O.; Juurlink; Stamouli, A.; Müller, M. A Molecular View of Cholesterol-Induced Condensation in a Lipid Monolayer. *J. Phys. Chem. B* **2004**, *108*, 19083–19085.

(46) Liu, J.; Conboy, J. C. Asymmetric Distribution of Lipids in a Phase Segregated Phospholipid Bilayer Observed by Sum-Frequency Vibrational Spectroscopy. *J. Phys. Chem. C* **2007**, *111*, 8988–8999.

(47) Ohe, C.; Goto, Y.; Noi, M.; Arai, M.; Kamijo, H.; Itoh, K. Sum Frequency Generation Spectroscopic Studies on Phase Transitions of Phospholipid Monolayers Containing Poly(Ethylene Oxide) Lipids at the Air-Water Interface. *J. Phys. Chem. B* **2007**, *111*, 1693–1700.

(48) Lis, D.; Guthmuller, J.; Champagne, B.; Humbert, C.; Busson, B.; Peremans, A.; Cecchet, F. Vibrational Sum-Frequency Generation Activity of a 2,4-Dinitrophenyl Phospholipid Hybrid Bilayer: Retrieving Orientational Parameters from a DFT Analysis of Experimental Data. *ChemPhysChem* **2013**, *14*, 1227–1236.

(49) Johnson, C. M.; Baldelli, S. Vibrational Sum Frequency Spectroscopy Studies of the Influence of Solutes and Phospholipids at Vapor/Water Interfaces Relevant to Biological and Environmental Systems. *Chem. Rev.* **2014**, *114*, 8416–8446.

(50) Li, B.; Lu, X.; Han, X.; Wu, F.-G.; Myers, J. N.; Chen, Z. Interfacial Fresnel Coefficients and Molecular Structures of Model Cell Membranes: From a Lipid Monolayer to a Lipid Bilayer. *J. Phys. Chem. C* **2014**, *118*, 28631–28639.

(51) Wei, F.; Xiong, W.; Li, W.; Lu, W.; Allen, H. C.; Zheng, W. Assembly and Relaxation Behaviours of Phosphatidylethanolamine Monolayers Investigated by Polarization and Frequency Resolved Sfg-Vs. *Phys. Chem. Chem. Phys.* **2015**, *17*, 25114–25122.

(52) Feng, R.-J.; Li, X.; Zhang, Z.; Lu, Z.; Guo, Y. Spectral Assignment and Orientational Analysis in a Vibrational Sum Frequency Generation Study of DPPC Monolayers at the Air/Water Interface. *J. Chem. Phys.* **2016**, *145*, 244707.

(53) Takeshita, N.; Okuno, M.; Ishibashi, T.-a. Molecular Conformation of DPPC Phospholipid Langmuir and Langmuir-Blodgett Monolayers Studied by Heterodyne-Detected Vibrational Sum Frequency Generation Spectroscopy. *Phys. Chem. Chem. Phys.* **2017**, *19*, 2060.

(54) Petersen, P. B.; Saykally, R. J.; Mucha, M.; Jungwirth, P. Enhanced Concentration of Polarizable Anions at the Liquid Water Surface: SHG Spectroscopy and MD Simulations of Sodium Thiocyanate. *J. Phys. Chem. B* **2005**, *109*, 10915–10921.

(55) Miller, A. E.; Petersen, P. B.; Hollars, C. W.; Saykally, R. J.; Heyda, J.; Jungwirth, P. Behavior of Beta-Amyloid 1–16 at the Air-Water Interface at Varying pH by Nonlinear Spectroscopy and

Molecular Dynamics Simulations. *J. Phys. Chem. A* **2011**, *115*, 5873–5880.

(56) Beierlein, F.; Krause, A.; Jaeger, C. M.; Fita, P.; Vauthey, E.; Clark, T. Molecular-Dynamics Simulations of Liquid Phase Interfaces: Understanding the Structure of the Glycerol/Water-Dodecane System. *Langmuir* **2013**, *29*, 11898–11907.

(57) Kundu, A.; Watanabe, H.; Yamaguchi, S.; Tahara, T. Agreement between Experimentally and Theoretically Estimated Orientational Distributions of Solutes at the Air/Water Interface. *J. Phys. Chem. C* **2013**, *117*, 8887–8891.

(58) Richert, S.; Mosquera Vazquez, S.; Grzybowski, M.; Gryko, D. T.; Kyrychenko, A.; Vauthey, E. Excited-State Dynamics of an Environment-Sensitive Push–Pull Diketopyrrolopyrrole: Major Differences between the Bulk Solution Phase and the Dodecane/Water Interface. *J. Phys. Chem. B* **2014**, *118*, 9952–9963.

(59) Loison, C.; Nasir, M. N.; Benichou, E.; Besson, F.; Brevet, P. F. Multi-Scale Modeling of Mycosubtilin Lipopeptides at the Air/Water Interface: Structure and Optical Second Harmonic Generation. *Phys. Chem. Chem. Phys.* **2014**, *16*, 2136–2148.

(60) Svechkarev, D.; Kolodezny, D.; Mosquera-Vazquez, S.; Vauthey, E. Complementary Surface Second Harmonic Generation and Molecular Dynamics Investigation of the Orientation of Organic Dyes at a Liquid/Liquid Interface. *Langmuir* **2014**, *30*, 13869–13876.

(61) Travkova, O. G.; Brezesinski, G. Adsorption of the Antimicrobial Peptide Arenicin and Its Linear Derivative to Model Membranes–a Maximum Insertion Pressure Study. *Chem. Phys. Lipids* **2013**, *167–168*, 43–50.

(62) Saint Martin, E.; Konovalov, O.; Daillant, J. Studies of Phospholipid Monolayer at Liquid/Liquid Interface in Presence of an Antimicrobial Peptide. *Thin Solid Films* **2007**, *515*, 5687–5690.

(63) Abraham, M. J.; Murtola, T.; Schulz, R.; Páll, S.; Smith, J. C.; Hess, B.; Lindahl, E. Gromacs: High Performance Molecular Simulations through Multi-Level Parallelism from Laptops to Supercomputers. *SoftwareX* **2015**, *1–2*, 19–25.

(64) Lindorff-Larsen, K.; Piana, S.; Palmo, K.; Maragakis, P.; Klepeis, J. L.; Dror, R. O.; Shaw, D. E. Improved Side-Chain Torsion Potentials for the Amber Ff99sb Protein Force Field. *Proteins: Struct., Funct., Genet.* **2010**, *78*, 1950–1958.

(65) Hornak, V.; Abel, R.; Okur, A.; Strockbine, B.; Roitberg, A.; Simmerling, C. Comparison of Multiple Amber Force Fields and Development of Improved Protein Backbone Parameters. *Proteins: Struct., Funct., Genet.* **2006**, *65*, 712–725.

(66) Jorgensen, W. L.; Chandrasekhar, J.; Madura, J. D.; Impey, R. W.; Klein, M. L. Comparison of Simple Potential Functions for Simulating Liquid Water. *J. Chem. Phys.* **1983**, *79*, 926–935.

(67) Jambeck, J. P.; Lyubartsev, A. P. An Extension and Further Validation of an All-Atomistic Force Field for Biological Membranes. *J. Chem. Theory Comput.* **2012**, *8*, 2938–2948.

(68) Jambeck, J. P.; Lyubartsev, A. P. Derivation and Systematic Validation of a Refined All-Atom Force Field for Phosphatidylcholine Lipids. *J. Phys. Chem. B* **2012**, *116*, 3164–3179.

(69) Wang, J.; Wang, W.; Kollman, P. A.; Case, D. A. Automatic Atom Type and Bond Type Perception in Molecular Mechanical Calculations. *J. Mol. Graphics Modell.* **2006**, *25*, 247–260.

(70) Singh, U. C.; Kollman, P. A. An Approach to Computing Electrostatic Charges for Molecules. *J. Comput. Chem.* **1984**, *5*, 129–145.

(71) Bayly, C. I.; Cieplak, P.; Cornell, W. D.; Kollman, P. A. A Well-Behaved Electrostatic Potential Based Method Using Charge Restraints for Deriving Atomic Charges: The RESP Model. *J. Phys. Chem.* **1993**, *97*, 10269–10280.

(72) Darden, T.; York, D.; Pedersen, L. Particle Mesh Ewald: An N X Log(N) Method for Ewald Sums in Large Systems. *J. Chem. Phys.* **1993**, *98*, 10089–10092.

(73) Hess, B.; Bekker, H.; Berendsen, H. J. C.; Fraaije, J. G. E. M. Lincs: A Linear Constraint Solver for Molecular Simulations. *J. Comput. Chem.* **1997**, *18*, 1463–1472.

(74) Miyamoto, S.; Kollman, P. A. Settle: An Analytical Version of the Shake and Rattle Algorithm for Rigid Water Models. *J. Comput. Chem.* **1992**, *13*, 952−962.

(75) Roux, B. The Calculation of the Potential of Mean Force Using Computer Simulations. *Comput. Phys. Commun.* **1995**, *91*, 275−282.

(76) Torrie, G. M.; Valleau, J. P. Nonphysical Sampling Distributions in Monte Carlo Free-Energy Estimation: Umbrella Sampling. *J. Comput. Phys.* **1977**, *23*, 187−199.

(77) Lemkul, J. A.; Bevan, D. R. Assessing the Stability of Alzheimer's Amyloid Protofibrils Using Molecular Dynamics. *J. Phys. Chem. B* **2010**, *114*, 1652−1660.

(78) Hub, J. S.; Winkler, F. K.; Merrick, M.; de Groot, B. L. Potentials of Mean Force and Permeabilities for Carbon Dioxide, Ammonia, and Water Flux across a Rhesus Protein Channel and Lipid Membranes. *J. Am. Chem. Soc.* **2010**, *132*, 13251−13263.

(79) Hub, J. S.; de Groot, B. L.; van der Spoel, D. G_Wham—a Free Weighted Histogram Analysis Implementation Including Robust Error and Autocorrelation Estimates. *J. Chem. Theory Comput.* **2010**, *6*, 3713−3720.

(80) Kumar, S.; Rosenberg, J. M.; Bouzida, D.; Swendsen, R. H.; Kollman, P. A. The Weighted Histogram Analysis Method for Free-Energy Calculations on Biomolecules. I. The Method. *J. Comput. Chem.* **1992**, *13*, 1011−1021.

(81) Frisch, M. J.; Trucks, G. W.; Schlegel, H. B.; Scuseria, G. E.; Robb, M. A.; Cheeseman, J. R.; Scalmani, G.; Barone, V.; Mennucci, B.; Petersson, G. A., et al. *Gaussian 09*, Revision D, Gaussian, Inc.: Wallingford, CT, 2009.

(82) Lee, C.; Yang, W.; Parr, R. G. Development of the Colle-Salvetti Correlation-Energy Formula into a Functional of the Electron Density. *Phys. Rev. B: Condens. Matter Mater. Phys.* **1988**, *37*, 785−789.

(83) Marenich, A. V.; Cramer, C. J.; Truhlar, D. G. Universal Solvation Model Based on Solute Electron Density and on a Continuum Model of the Solvent Defined by the Bulk Dielectric Constant and Atomic Surface Tensions. *J. Phys. Chem. B* **2009**, *113*, 6378−6396.

(84) Bauernschmitt, R.; Ahlrichs, R. Treatment of Electronic Excitations within the Adiabatic Approximation of Time Dependent Density Functional Theory. *Chem. Phys. Lett.* **1996**, *256*, 454−464.

(85) Stratmann, R. E.; Scuseria, G. E.; Frisch, M. J. An Efficient Implementation of Time-Dependent Density-Functional Theory for the Calculation of Excitation Energies of Large Molecules. *J. Chem. Phys.* **1998**, *109*, 8218−8224.

(86) Scalmani, G.; Frisch, M. J.; Mennucci, B.; Tomasi, J.; Cammi, R.; Barone, V. Geometries and Properties of Excited States in the Gas Phase and in Solution: Theory and Application of a Time-Dependent Density Functional Theory Polarizable Continuum Model. *J. Chem. Phys.* **2006**, *124*, 094107.

(87) Yanai, T.; Tew, D. P.; Handy, N. C. A New Hybrid Exchange-Correlation Functional Using the Coulomb-Attenuating Method (CAM-B3LYP). *Chem. Phys. Lett.* **2004**, *393*, 51−57.

(88) Castro, A.; Bhattacharyya, K.; Eisenthal, K. B. Energetics of Adsorption of Neutral and Charged Molecules at the Air/Water Interface by Second Harmonic Generation: Hydrophobic and Solvation Effects. *J. Chem. Phys.* **1991**, *95*, 1310−1315.

(89) Song, J.; Kim, M. W. Second Harmonic Generation Study of Malachite Green Adsorption at the Interface between Air and an Electrolyte Solution: Observing the Effect of Excess Electrical Charge Density at the Interface. *J. Phys. Chem. B* **2010**, *114*, 3236−3241.

(90) Subir, M.; Eltouny, N.; Ariya, P. A. A Surface Second Harmonic Generation Investigation of Volatile Organic Compound Adsorption on a Liquid Mercury Surface. *RSC Adv.* **2015**, *5*, 23464−23470.

(91) Limousin, G.; Gaudet, J. P.; Charlet, L.; Szenknect, S.; Barthès, V.; Krimissa, M. Sorption Isotherms: A Review on Physical Bases, Modeling and Measurement. *Appl. Geochem.* **2007**, *22*, 249−275.

(92) Higgins, D. A.; Byerly, S. K.; Abrams, M. B.; Corn, R. M. Second Harmonic Generation Studies of Methylene Blue Orientation at Silica Surfaces. *J. Phys. Chem.* **1991**, *95*, 6984−6990.

(93) Neumann, B.; Pollmann, P. Investigation of Two Cyanine Dyes at Normal and High Pressure by UV/Vis Spectroscopy. *Phys. Chem. Chem. Phys.* **2000**, *2*, 4784−4792.

(94) Chibisov, A. K. Photonics of Dimers of Cyanine Dyes. *High Energy Chem.* **2007**, *41*, 200−209.

(95) Ahmadi, S.; Deligeorgiev, T. G.; Vasilev, A.; Kubista, M. The Dimerization Study of Some Cationic Monomethine Cyanine Dyes by Chemometrics Method. *Russ. J. Phys. Chem. A* **2012**, *86*, 1974−1981.

(96) Vacha, R.; Roke, S. Sodium Dodecyl Sulfate at Water−Hydrophobic Interfaces: A Simulation Study. *J. Phys. Chem. B* **2012**, *116*, 11936−11942.

(97) Yamaguchi, S.; Tahara, T. Heterodyne-Detected Electronic Sum Frequency Generation: "Up" Versus "Down" Alignment of Interfacial Molecules. *J. Chem. Phys.* **2008**, *129*, 101102.

(98) Nihonyanagi, S.; Mondal, J. A.; Yamaguchi, S.; Tahara, T. Structure and Dynamics of Interfacial Water Studied by Heterodyne-Detected Vibrational Sum-Frequency Generation. *Annu. Rev. Phys. Chem.* **2013**, *64*, 579−603.

(99) Rao, Y.; Hong, S.-Y.; Turro, N. J.; Eisenthal, K. B. Molecular Orientational Distribution at Interfaces Using Second Harmonic Generation. *J. Phys. Chem. C* **2011**, *115*, 11678−11683.

(100) Rusch, P. F.; Lelieur, J. P. Analytical Moments of Skewed Gaussian Distribution Functions. *Anal. Chem.* **1973**, *45*, 1541−1543.

(101) Lerner, R. A.; Meinke, W.; Goldstein, D. A. Membrane-Associated DNA in the Cytoplasm of Diploid Human Lymphocytes. *Proc. Natl. Acad. Sci. U. S. A.* **1971**, *68*, 1212−1216.

(102) Cheng, J.; Torkamani, A.; Peng, Y.; Jones, T. M.; Lerner, R. A. Plasma Membrane Associated Transcription of Cytoplasmic DNA. *Proc. Natl. Acad. Sci. U. S. A.* **2012**, *109*, 10827−10831.